ISSN No:-2456-2165 https://doi.org/10.38124/ijisrt/26apr1449

Machine Learning-Assisted Optimization of Fractal-Based Multi-Band MIMO Antenna for Wireless Applications

Sri Chandrika Naidu[1]; Balaji Pachharu[2]; Mahanwith Karanam[3]; Saidu Babu Kumbha[4]

[1,2,3,4]Student, Department of Electronics and Communication Engineering, R.V.R. & J.C. College of Engineering, Guntur, Andhra Pradesh, India

Publication Date: 2026/04/30

Abstract—This paper presents the design, simulation, and machine learning-assisted optimization of a compact multi-band MIMO antenna incorporating fractal geometry. Multi-band MIMO antennas play a vital role in modern wireless communication systems by enabling operation across multiple frequency bands while maintaining high data rates and reliable performance. However, designing compact multi-band antennas with stable impedance matching, high isolation, and consistent radiation characteristics remains a challenging task. To address these challenges, a fractal-based antenna structure is employed, where the self-similar geometry enhances multi-band behavior and improves space utilization. Machine learning models are utilized to predict the reflection coefficient (|S11|) based on antenna design parameters, thereby reducing dependency on repeated full-wave simulations. Further optimization is carried out using Particle Swarm Optimization (PSO) and Moth-Flame Optimization (MFO) algorithms to enhance bandwidth and overall antenna performance. The proposed approach improves computational efficiency, supports antenna miniaturization, and achieves accurate prediction of optimal design parameters. The optimized multi-band MIMO antenna demonstrates improved reflection characteristics and stable performance, making it suitable for high-performance wireless communication applications.

Keywords: *Multi-Band MIMO Antenna, Fractal Geometry, Machine Learning, Antenna Optimization, Gaussian Process Regression, Random Forest Regression, Particle Swarm Optimization, Moth-Flame Optimization, Reflection Coefficient (|S_{11}|).*

How to Cite: Sri Chandrika Naidu; Balaji Pachharu; Mahanwith Karanam; Saidu Babu Kumbha (2026) Machine Learning-Assisted Optimization of Fractal-Based Multi-Band MIMO Antenna for Wireless Applications.
International Journal of Innovative Science and Research Technology, 11(4), 2575-2587.
https://doi.org/10.38124/ijisrt/26apr1449

I. INTRODUCTION

➢ *The Imperative for Multi-Band MIMO Architectures*

The relentless evolution of wireless communication ecosystems has precipitated an unprecedented demand for spectral agility and spatial diversity in antenna systems. Multi-band Multiple-Input Multiple-Output (MIMO) configurations have emerged as indispensable enablers for contemporary wireless standards, including Fifth Generation New Radio (5G NR), IEEE 802.11ax (Wi-Fi 6), and evolving cellular paradigms. These architectures facilitate concurrent operation across disparate frequency bands, thereby augmenting spectral efficiency, enhancing link reliability, and accommodating the exponential throughput requirements of modern applications [1].

The application landscape for compact multi-band MIMO radiators encompasses handheld mobile terminals, cellular base station infrastructure, Internet of Things (IoT) gateways, and vehicular communication systems. In each domain, the imperative for concurrent multi-band operation collides with stringent volumetric constraints, necessitating innovative approaches to antenna miniaturization without commensurate performance degradation.

➢ *Design Challenges in Compact Multi-Band Radiators*

The realization of compact multi-band MIMO antennas confronts several formidable technical challenges that have persisted as active research frontiers in the electromagnetic community:

- Impedance Matching Complexity: Achieving stable impedance characteristics across multiple frequency bands requires intricate geometric tailoring. The impedance bandwidth must accommodate disparate operational frequencies while maintaining $|S_{11}| < -10$ dB, demanding sophisticated matching network design or inherent broadband structural properties.

ISSN No:-2456-2165 https://doi.org/10.38124/ijisrt/26apr1449

- Mutual Coupling in Spatially Constrained Arrays: The proximity of radiating elements in compact configurations engenders undesirable electromagnetic coupling, manifesting as degraded isolation (S_{21}) and compromised diversity performance. Maintaining isolation below −15 dB while preserving miniaturization presents a fundamental physical trade-off.
- Pattern Stability Versus Frequency: The radiation characteristics must remain consistent across the operational spectrum to ensure reliable communication. Pattern degradation at specific frequencies can create coverage gaps, undermining the multi-band operational mandate.
- Miniaturization-Radiation Efficiency Trade-offs: The Chu-Harrington limit establishes fundamental bounds on the relationship between antenna size and bandwidth efficiency. Miniaturization efforts must navigate these physical constraints while preserving acceptable radiation efficiency.

➢ *Fractal Electromagnetics: A Paradigm for Miniaturization*

Fractal geometry, conceived by Mandelbrot [2], offers an elegant mathematical framework for addressing the miniaturization challenge while simultaneously enabling multi-band resonance. The space-filling topology of iterated function systems facilitates electrical current path extension within constrained physical volumes, effectively decoupling electrical size from physical dimensions.

The Koch snowflake, a canonical fractal structure, is generated through iterative application of the Koch curve construction to each side of an equilateral triangle. After n iterations, the total curve length evolves according to:

$$L_n = L_o \times (4/3)^n \quad (1)$$

The Hausdorff fractal dimension D_f, characterizing the space-filling properties, is calculated as:

$$Df = \log(4)/\log(3) \approx 1.2618 \quad (2)$$

This non-integer dimension, intermediate between a one-dimensional line (D=1) and a two-dimensional plane (D=2), engenders the multi-scale current distribution that supports concurrent multi-band operation.

➢ *Computational Challenges and Machine Learning Solutions*

Traditional antenna optimization relies upon computationally expensive parametric sweeps or manual tuning by experienced designers. Full-wave electromagnetic simulations, employing finite-difference time-domain (FDTD) or finite-element method (FEM) formulations, typically require approximately four minutes per iteration. A comprehensive 10×10×10 parameter sweep would necessitate 1,000 simulation runs, consuming approximately 66.7 hours—a duration incompatible with modern design cycle requirements.

Machine learning offers a paradigm shift through the construction of surrogate models that approximate the electromagnetic response space with remarkable fidelity [3]. Gaussian Process Regression (GPR) and Random Forest Regression (RFR) have emerged as particularly effective methodologies, offering complementary strengths in uncertainty quantification and robustness to overfitting, respectively.

➢ *Novel Contributions*

This manuscript presents several distinctive contributions to the state-of-the-art:

- A fractal-based multi-band MIMO topology incorporating Koch snowflake-inspired radiating elements, achieving enhanced spectral agility within compact volumetric constraints.
- A rigorous comparative study of GPR and RFR surrogate methodologies for antenna response prediction, with quantitative performance characterization.
- A systematic evaluation of PSO and MFO algorithms for antenna design optimization, establishing the superiority of the MFO-GPR combination.
- Empirical validation through a 20-point experimental design, demonstrating 97.6% reduction in computational time relative to conventional parameter sweep approaches.

II. ANTENNA DESIGN AND FRACTAL GEOMETRY

➢ *Mathematical Foundations of Fractal Antennas*

The theoretical underpinnings of fractal antenna engineering rest upon the concept of self-similarity. The Koch curve, introduced by Helge von Koch in 1904, exemplifies this property through its recursive generation process. The fractal dimension D_f quantifies the space-filling capacity through:

$$Df = \log(N)/\log(1/r) \quad (3)$$

Where N represents the number of self-similar copies and r denotes the scaling factor. For the Koch curve, N=4 and r=1/3, yielding $D_f \approx 1.2618$.

➢ *Geometric Configuration*

The proposed antenna comprises a 1×2 MIMO configuration with Koch snowflake-inspired hexagonal radiating elements positioned on a Roger RO4003C substrate. The substrate specifications are:

- Dielectric constant: $\varepsilon_r = 3.38$
- Loss tangent: $\tan\delta = 0.0027$
- Thickness: h = 1.6 mm
- Copper cladding: 35 μm with conductivity $\sigma = 5.8\times10^7$ S/m

The feeding structure employs Coplanar Waveguide (CPW) configuration with 50 Ω characteristic impedance, offering advantages in reduced dispersion, simplified

ISSN No:-2456-2165 https://doi.org/10.38124/ijisrt/26apr1449

fabrication, and seamless integration with planar circuit elements.

➢ *Design Parameterization*

The optimization framework identifies three critical geometric parameters:

- x: Overall scaling parameter governing the antenna footprint, ranging from 10 mm to 13 mm.
- wf: Feed line width affecting impedance matching and current distribution, ranging from 2 mm to 4 mm.
- a: Fractal iteration scaling factor controlling the geometric complexity and multi-band resonance characteristics, ranging from 2 mm to 4 mm.

➢ *CST Microwave Studio Implementation*

The electromagnetic simulations were conducted using CST Studio Suite 2025 with the Time Domain Solver. The antenna front view is depicted in Fig. 1, the rear view in Fig. 2, the side profile in Fig. 3, and the three-dimensional visualization in Fig. 4. The solver employs hexahedral mesh with adaptive refinement, absorbing boundary conditions with PML termination, and waveguide port excitation with 50 Ω reference impedance.

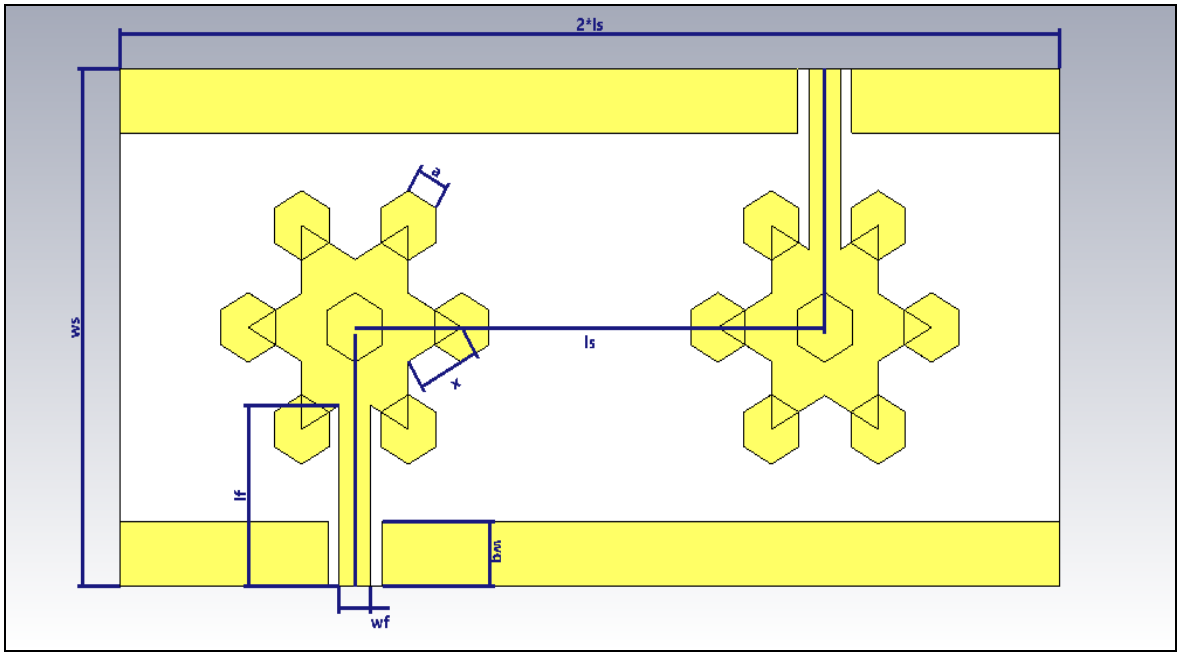

Fig 1 Front view of the Proposed Fractal-Based Multi-Band MIMO Antenna Showing Koch Snowflake-Inspired Hexagonal Radiating Elements with Geometric Parameter Annotations.

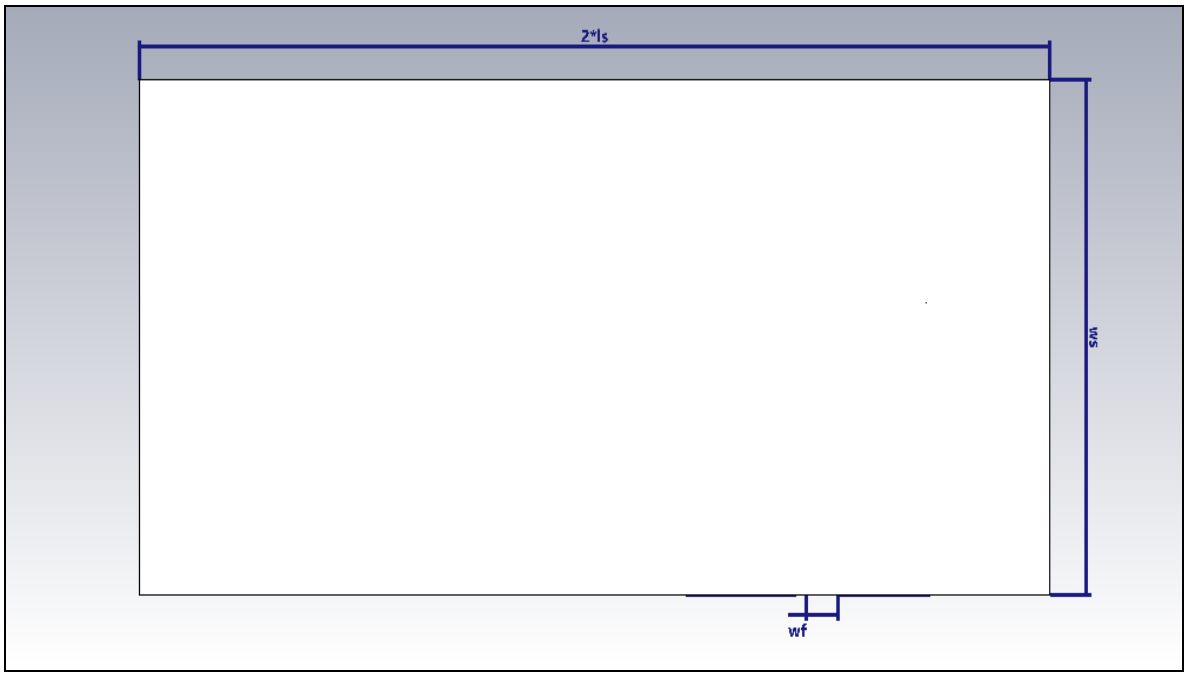

Fig 2 Rear view Illustrating the Partial Ground Plane Configuration and Coplanar Waveguide Feeding Mechanism.

ISSN No:-2456-2165 https://doi.org/10.38124/ijisrt/26apr1449

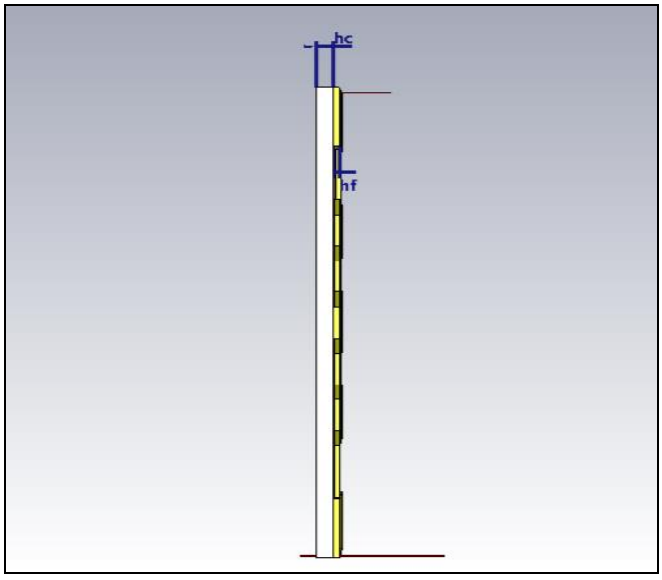

Fig 3 Side view Depicting the Multilayer Substrate Configuration with 1.6 mm Roger RO4003C and Copper Cladding Thickness.

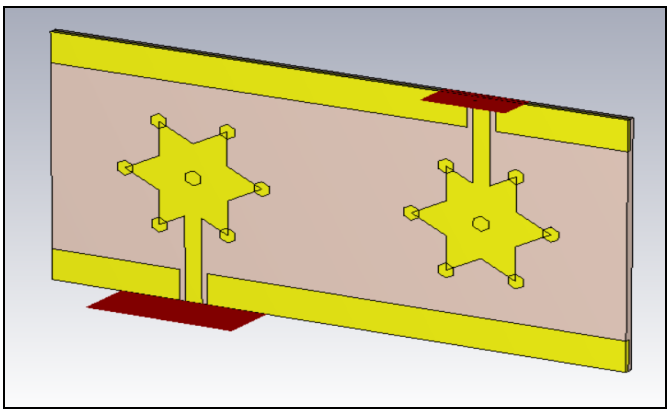

Fig 4 Three-Dimensional Isometric view of the Complete 1×2 MIMO Antenna Configuration Showing Element Arrangement and Feeding Network.

III. SURROGATE-ASSISTED OPTIMIZATION FRAMEWORK

➢ *The Surrogate Modeling Paradigm*

The computational burden associated with full-wave electromagnetic simulation presents a fundamental bottleneck. Each CST simulation requires approximately four minutes. A conventional 10×10×10 parameter sweep would require 1,000 simulations—approximately 66.7 hours. Surrogate modeling constructs mathematical approximations of the expensive simulation response, enabling millisecond-level prediction.

➢ *B. Experimental Design for Training Data Generation*

The training dataset comprises 20 simulation runs generated through uniform random sampling across the three-dimensional parameter space: x ∈ [10, 13] mm, wf ∈ [2, 4] mm, and a ∈ [2, 4] mm. The CST-Python automation framework leverages the COM API to enable seamless parameter modification and result extraction. A VBA script facilitates dynamic geometry updates:

```
Sub Main()

StoreParameter "x", 12.35

StoreParameter "wf", 3.12

StoreParameter "a", 3.45

Rebuild

Solver.Start

End Sub
```

➢ *Gaussian Process Regression Methodology*

Gaussian Process Regression (GPR) provides a non-parametric Bayesian framework for function approximation, offering the distinct advantage of uncertainty quantification alongside point predictions. The Radial Basis Function (RBF) kernel with Automatic Relevance Determination (ARD) was selected:

$$k(x, x') = \sigma^2 f \exp(-\tfrac{1}{2}(x-x')^T \Lambda^{-1}(x-x')) \quad (4)$$

Hyperparameter optimization was performed through marginal likelihood maximization, yielding a training set coefficient of determination $R^2 = 0.94$.

➢ *Random Forest Regression Approach*

Random Forest Regression (RFR) constructs an ensemble of 200 decision trees through bootstrap aggregation (bagging), offering robustness to overfitting and implicit feature selection. The ensemble prediction aggregates individual tree outputs through averaging, yielding $R^2 = 0.96$. Feature importance analysis reveals: x (38%), a (35%), and wf (27%).

➢ *Particle Swarm Optimization Theory*

Particle Swarm Optimization (PSO) emulates the social behavior of biological swarms. Each particle i evolves according to:

$$v_i(t+1) = wv_i(t) + c_1r_1(p\_best,i - x_i(t)) + c_2r_2(g\_best - x_i(t)) \quad (5)$$

$$x_i(t+1) = x_i(t) + v_i(t+1) \quad (6)$$

The swarm comprised 20 particles evolved over 30 iterations with $w = 0.7$, $c_1 = c_2 = 1.5$.

➢ *Moth-Flame Optimization Principles*

Moth-Flame Optimization (MFO) draws inspiration from the transverse orientation navigation mechanism of nocturnal moths. The mathematical model employs a logarithmic spiral trajectory:

$$M_i = D_i \cdot e\text{^}(bt) \cdot \cos(2\pi t) + Flamej \quad (7)$$

$$|Flames| = round(N - t \cdot (N-1)/T) \quad (8)$$

The population comprised 10 moths evolved over 20 iterations.

ISSN No:-2456-2165 https://doi.org/10.38124/ijisrt/26apr1449

➢ *MIMO Performance Metrics Computation*

The optimization objective integrates multiple performance criteria. The constituent metrics are computed as follows:

- *Envelope Correlation Coefficient (ECC):*

$$ECC = |S^*_{11}S_{12} + S^*_{21}S_{22}|^2 / [(1-|S_{11}|^2-|S_{21}|^2)(1-|S_{22}|^2-|S_{12}|^2)] \quad (9)$$

Requirement: ECC < 0.5

- *Diversity Gain (DG):*

$$DG = 10\sqrt{(1 - ECC^2)}\ [dB] \quad (10)$$

Target: DG ≈ 10 dB

- *Channel Capacity Loss (CCL):*

$$CCL = -\log_2(1 - ECC^2)\ [bits/s/Hz] \quad (11)$$

Requirement: CCL < 0.4 bits/s/Hz

- *Total Active Reflection Coefficient (TARC):*

$$TARC = 20\log_{10}(\sqrt{((|S_{11}|^2+|S_{21}|^2)/2)})\ [dB] \quad (12)$$

Target: TARC < −10 dB

➢ *Fitness Function Design*

The multi-objective fitness function aggregates performance metrics through weighted summation:

$$\mathcal{F} = \bar{S}_{11} + 0.3\cdot ISO + 5.0\cdot ECC + 0.5\cdot CCL + 0.2\cdot TARC \quad (13)$$

Where $\bar{S}_{11}$ denotes the mean reflection coefficient, ISO represents isolation. The elevated weight (5.0) assigned to ECC underscores the primacy of diversity performance in MIMO applications.

IV. EMPIRICAL RESULTS AND ANALYSIS

➢ *Training Dataset Characterization*

The initial experimental design comprised 20 simulation runs uniformly sampling the parameter space. Table I presents the comprehensive dataset with measured performance metrics. Statistical analysis reveals:

- ECC range: 0.0113 to 0.0247 (mean: 0.0163, σ: 0.0035)
- DG range: 9.987 to 9.998 dB (mean: 9.994 dB)
- CCL range: 0.0007 to 0.0037 bits/s/Hz
- Isolation range: −32.42 to −25.88 dB

Table 1 Training Dataset: Initial 20 Simulation Runs

Run	x (mm)	wf (mm)	a (mm)	S11 (dB)	Isolation (dB)	ECC	DG (dB)	CCL
1	11.08	3.68	2.13	−6.51	−26.29	0.0121	9.997	0.0007
2	11.91	2.16	2.16	−5.92	−29.18	0.0208	9.992	0.0022
3	11.09	3.69	3.16	−6.82	−28.81	0.0123	9.997	0.0008
4	11.10	2.54	2.51	−6.72	−28.16	0.0179	9.994	0.0016
5	12.78	2.32	2.66	−5.72	−31.44	0.0204	9.991	0.0026
6	12.81	3.70	3.17	−5.10	−31.14	0.0131	9.995	0.0014
7	10.44	3.69	2.22	−6.94	−25.88	0.0122	9.997	0.0008
8	11.62	3.45	3.13	−6.46	−29.53	0.0135	9.996	0.0011
9	11.56	2.69	4.00	−6.95	−30.71	0.0178	9.992	0.0024
10	11.40	3.93	2.06	−6.02	−26.45	0.0113	9.998	0.0007
11	12.92	2.00	2.53	−5.23	−32.42	0.0247	9.987	0.0037
12	11.31	3.31	3.74	−6.88	−30.24	0.0139	9.996	0.0013
13	10.48	2.11	2.21	−5.82	−27.35	0.0205	9.993	0.0020
14	12.49	2.67	3.08	−6.18	−31.06	0.0179	9.992	0.0022
15	11.79	3.01	3.81	−6.86	−30.79	0.0159	9.993	0.0019
16	12.67	2.42	2.62	−5.84	−31.02	0.0193	9.992	0.0023
17	11.33	2.26	2.80	−6.47	−30.00	0.0209	9.992	0.0023
18	12.64	3.01	3.61	−5.88	−31.49	0.0165	9.992	0.0024
19	11.19	2.88	2.77	−6.73	−28.51	0.0157	9.996	0.0013
20	10.91	2.93	3.06	−6.90	−29.08	0.0156	9.996	0.0013

➢ *ML Optimization Run Analysis: All 20 Simulation Runs*

Fig. 5 presents the grouped bar chart of MIMO metrics with threshold indicators across all 20 simulation runs. The dashed threshold lines confirm that ECC, DG, and CCL consistently satisfy their respective design requirements. The Isolation values remain well below −15 dB in all runs, while VSWR exhibits greater variability, with run 10 recording the highest value of approximately 31.

ISSN No:-2456-2165 https://doi.org/10.38124/ijisrt/26apr1449

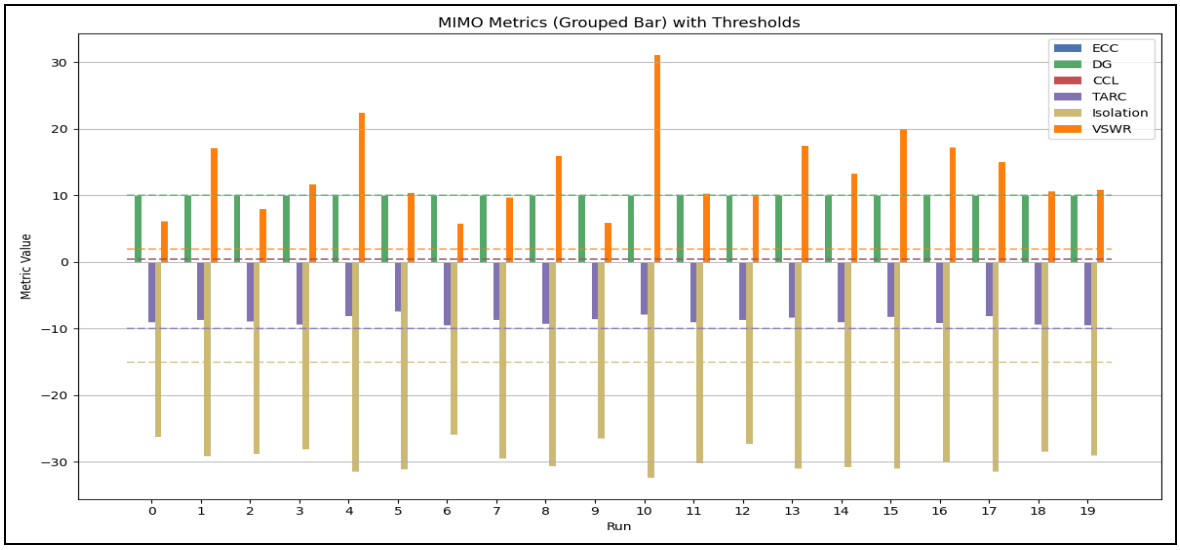

Fig 5 MIMO Metrics Grouped Bar Chart for all 20 Initial Simulation Runs, with Threshold Lines Indicating Design Requirements for ECC (< 0.5), DG (∼10 dB), CCL (< 0.4 bits/s/Hz), TARC (< −10 dB), Isolation (< −15 dB), and VSWR.

Fig. 6 further decomposes the metric evolution across all 20 runs into individual subplots. The ECC subplot confirms that all runs achieve values far below the 0.5 threshold (range: 0.011 to 0.025). The VSWR subplot exposes significant variability, emphasizing its role as the most sensitive metric to parameter selection.

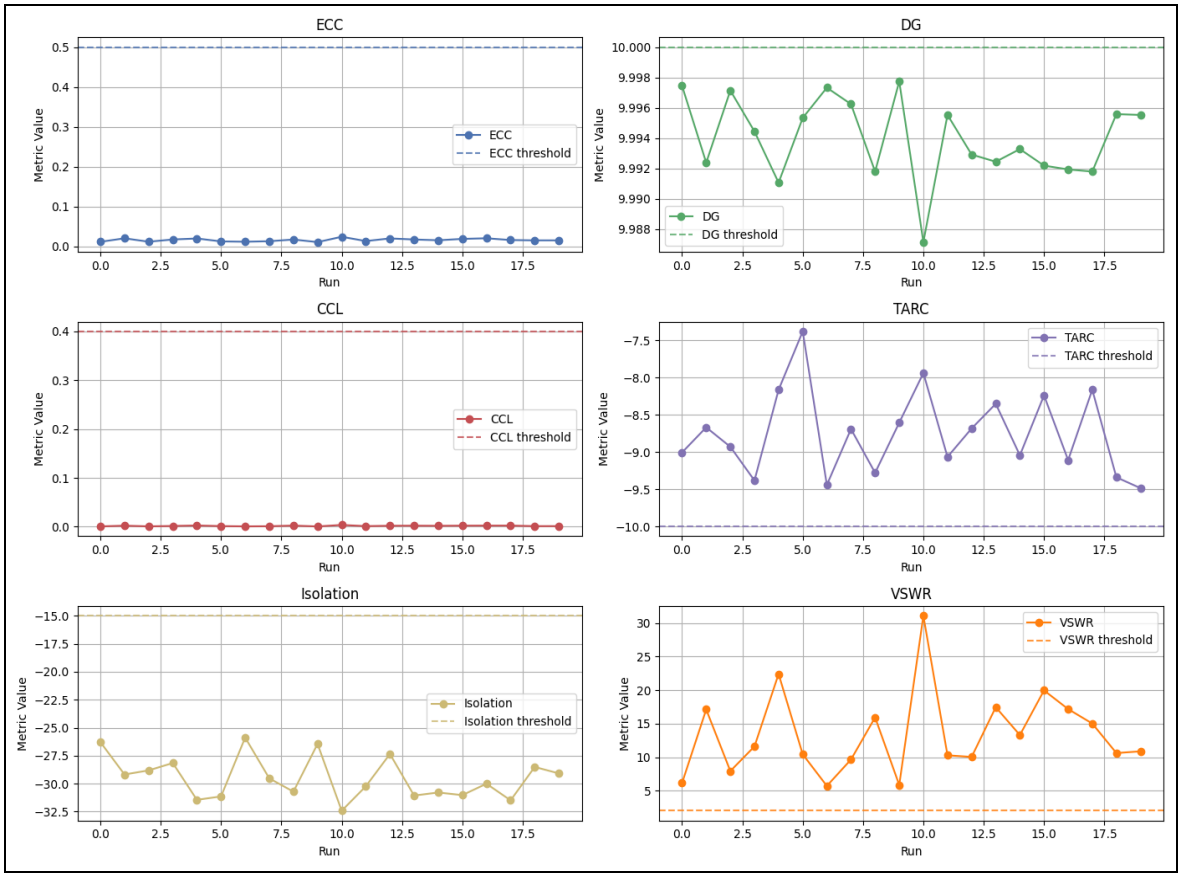

Fig 6 Individual Metric Subplots for all 20 Simulation Runs: ECC, DG, CCL, TARC, Isolation, and VSWR, Each Shown with their Respective Threshold Lines.

➢ *ML-Predicted Optimal Design: MIMO Metrics Analysis*

Figs. 7 and 8 present the MIMO metrics for the four ML-optimized configurations (PSO+GPR, PSO+RFR, MFO+GPR, MFO+RFR). The MFO+GPR configuration achieves the most balanced performance: ECC of 0.0137, DG of 9.996 dB, and isolation of −29.72 dB. In contrast, MFO+RFR yields superior isolation (−37.23 dB) but exhibits the worst VSWR (20.40) and a degraded $|S_{11}|$ of only −3.21 dB.

ISSN No:-2456-2165 https://doi.org/10.38124/ijisrt/26apr1449

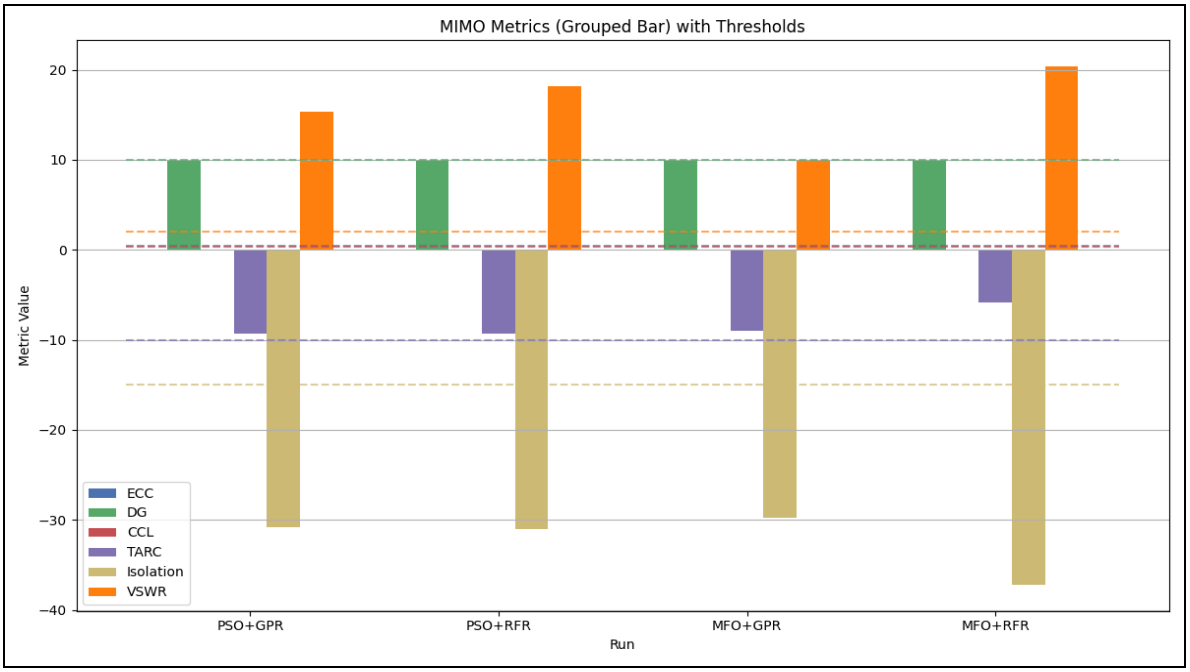

Fig 7 MIMO Metrics Grouped Bar Chart for the Four ML-Optimized Configurations: PSO+GPR, PSO+RFR, MFO+GPR, and MFO+RFR. Threshold Lines are Overlaid for Direct Compliance Verification.

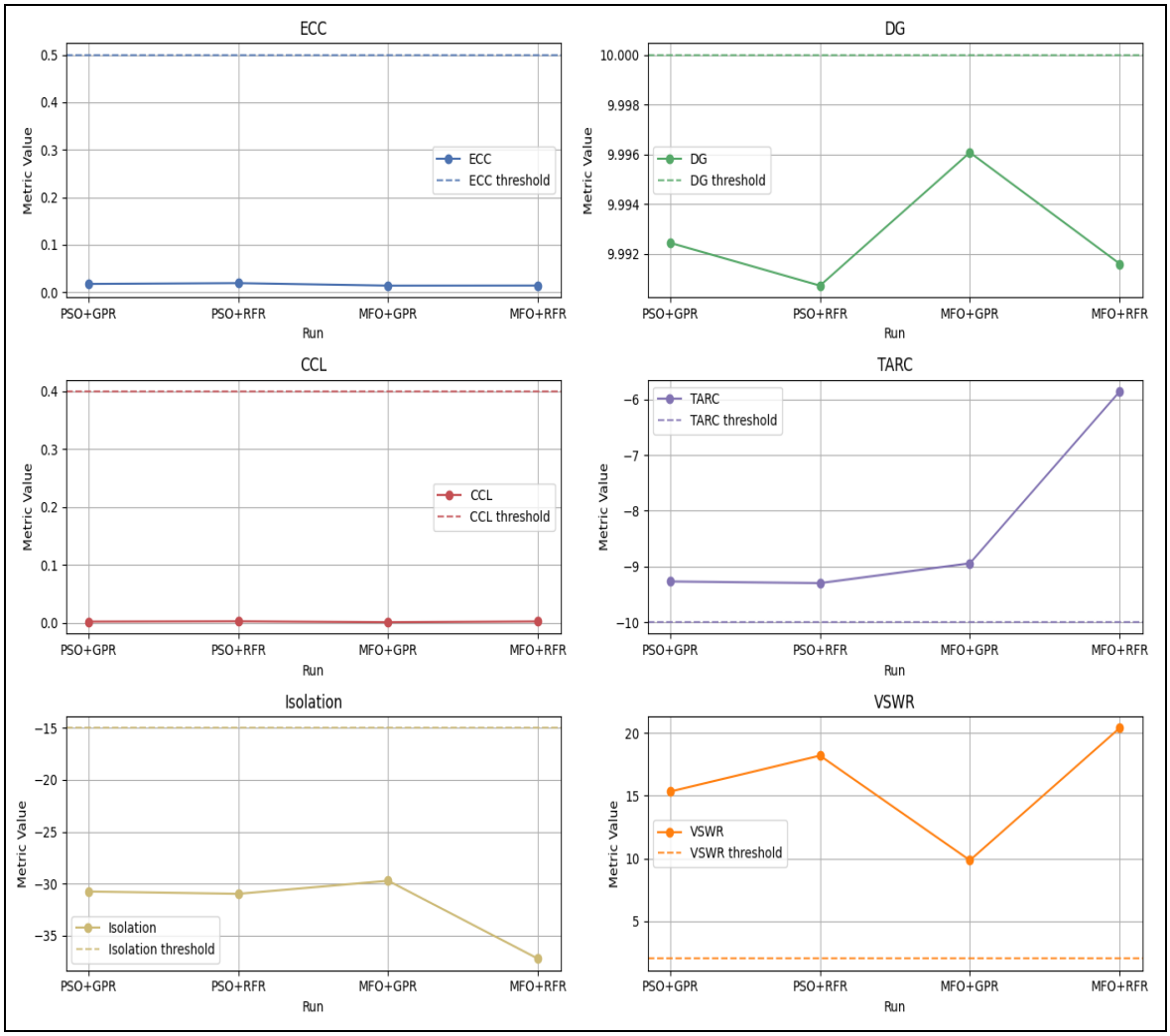

Fig 8 Individual Metric Subplots for the Four ML-Optimized Runs: (a) ECC, (b) DG, (c) CCL, (d) TARC, (e) Isolation, (f) VSWR. MFO+GPR Achieves the Optimal Trade-off Across all Metrics.

ISSN No:-2456-2165 https://doi.org/10.38124/ijisrt/26apr1449

➢ *S-Parameter Analysis of Optimized Configurations*

Figs. 9 through 14 present the S11 (Return Loss) and Isolation (S21) frequency responses for the key simulation runs, spanning 3 GHz to 12 GHz, with reference thresholds at |S11| < −10 dB and Isolation < −15 dB overlaid.

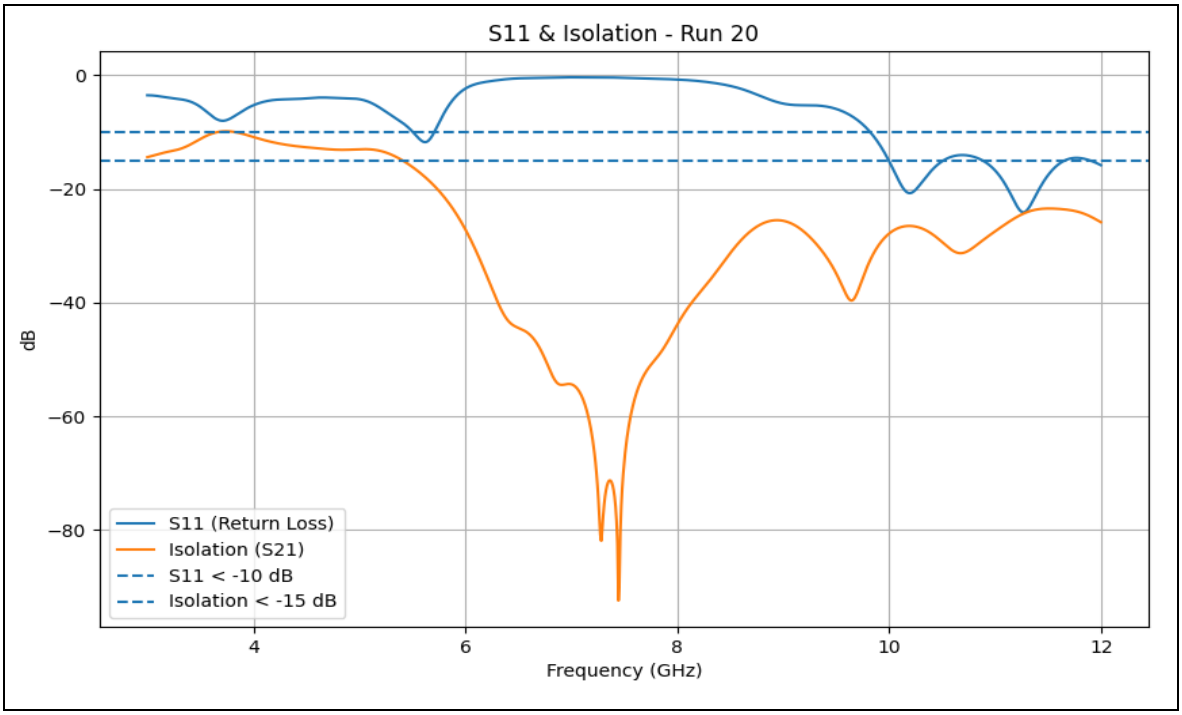

Fig 9 S11 and Isolation Frequency Response for the 20th (Final) Initial Simulation Run. The Antenna Exhibits Multi-Band Resonance with Deep Isolation Nulls Around 7.5 GHz (< −80 dB).

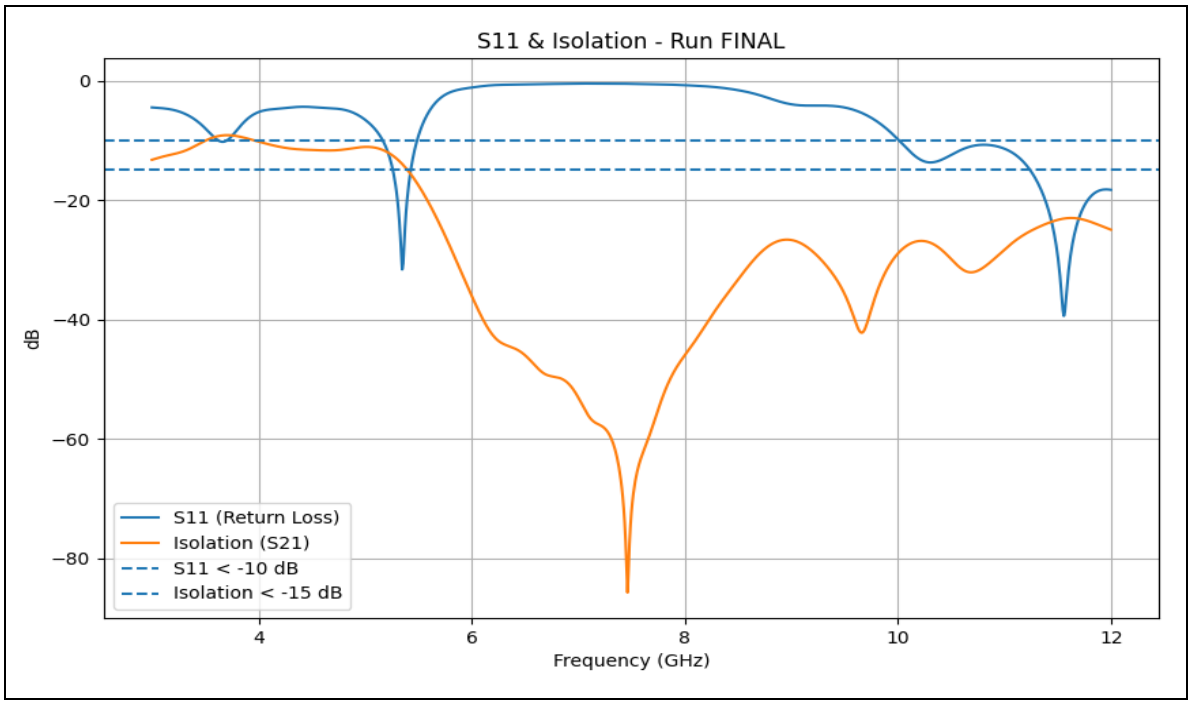

Fig 10 S11 and Isolation for the Final ML-Optimized Design (MFO+GPR), Confirming Broad Wideband Isolation and Multi-Band S11 Resonance Behavior.

ISSN No:-2456-2165 https://doi.org/10.38124/ijisrt/26apr1449

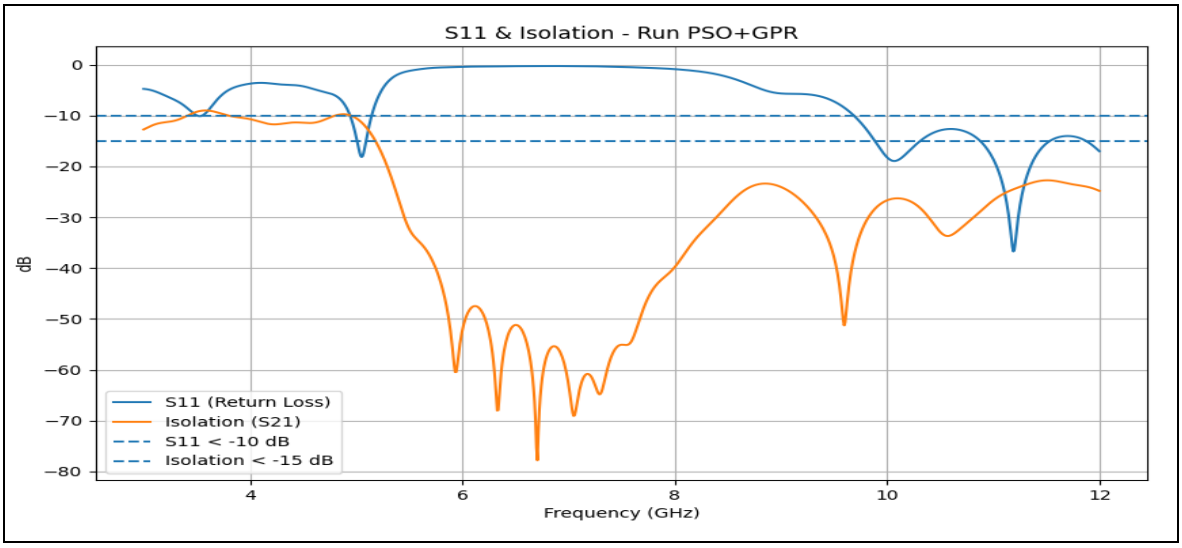

Fig 11 S11 and Isolation for the PSO+GPR Optimized Design. Good Isolation (< −15 dB) is Maintained Across Most of the Band.

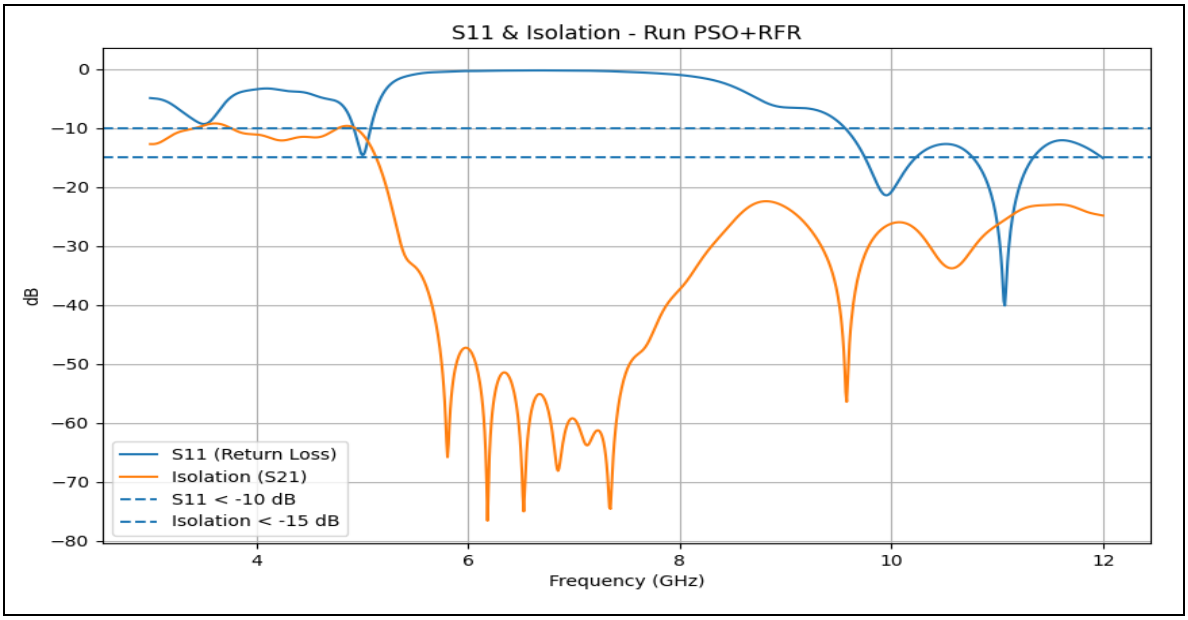

Fig 12 S11 and Isolation for the PSO+RFR Optimized Design, Exhibiting Comparable Behavior to PSO+GPR with Slightly Deeper Isolation Notches in the Mid-Band Region.

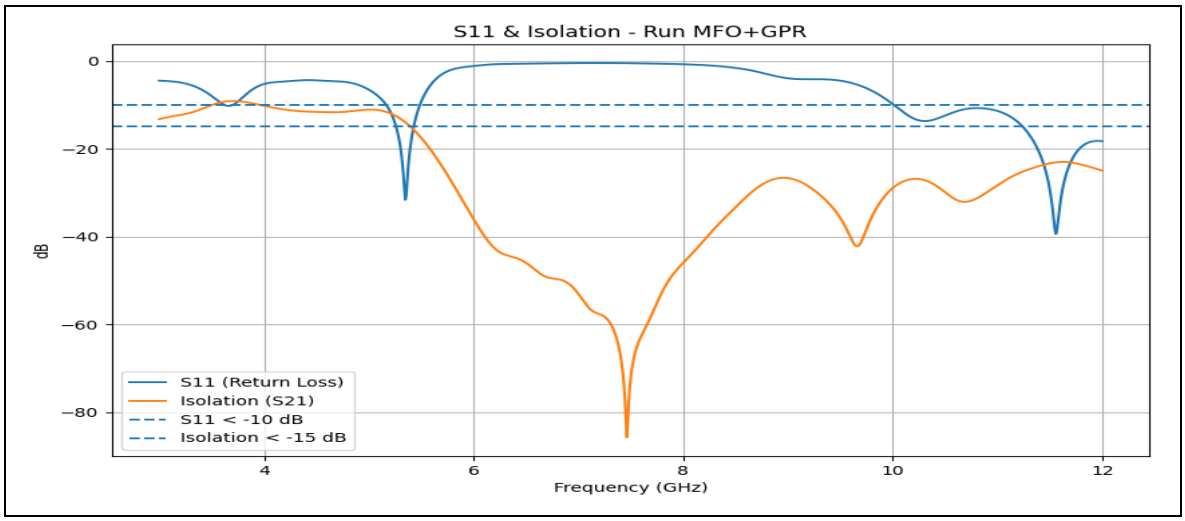

Fig 13 S11 and Isolation for the MFO+GPR Optimized Design — the Best-Performing Configuration. Deep Isolation Nulls Around 7.5 GHz Confirm MFO+GPR as the Superior Optimization Strategy.

ISSN No:-2456-2165 https://doi.org/10.38124/ijisrt/26apr1449

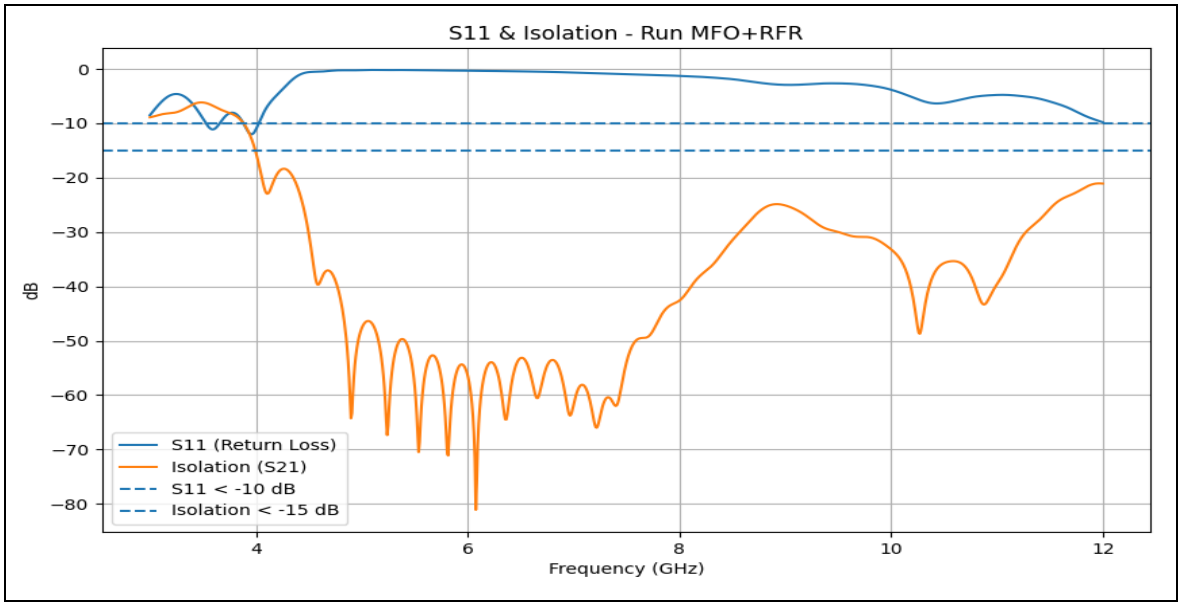

Fig 14 S11 and Isolation for the MFO+RFR Optimized Design. While Isolation is Excellent, the S11 Performance is Severely Degraded Above 4 GHz.

Table 2 Complete ML Optimization Results: All Performance Metrics

Method	S11 (dB)	Isolation (dB)	ECC	TARC (dB)	VSWR	DG (dB)
PSO+GPR	−6.93	−30.75	0.0173	−9.27	15.33	9.992
PSO+RFR	−6.88	−30.98	0.0190	−9.30	18.19	9.991
MFO+GPR	**−6.78**	**−29.72**	**0.0137**	**−8.94**	**9.85**	**9.996**
MFO+RFR	−3.21	−37.23	0.0139	−5.86	20.40	9.992
Threshold	< −10	< −15	< 0.5	< −10	< 2	~10

➢ *Electromagnetic Performance Evaluation*

Fig. 15 illustrates the simulated S-parameters of the antenna configuration. The reflection coefficient $|S_{11}|$ exhibits multi-band resonance characteristics with distinct minima corresponding to the fractal-induced harmonics. The mutual coupling $|S_{21}|$ remains below −25 dB across the operational spectrum, indicating excellent isolation between MIMO elements.

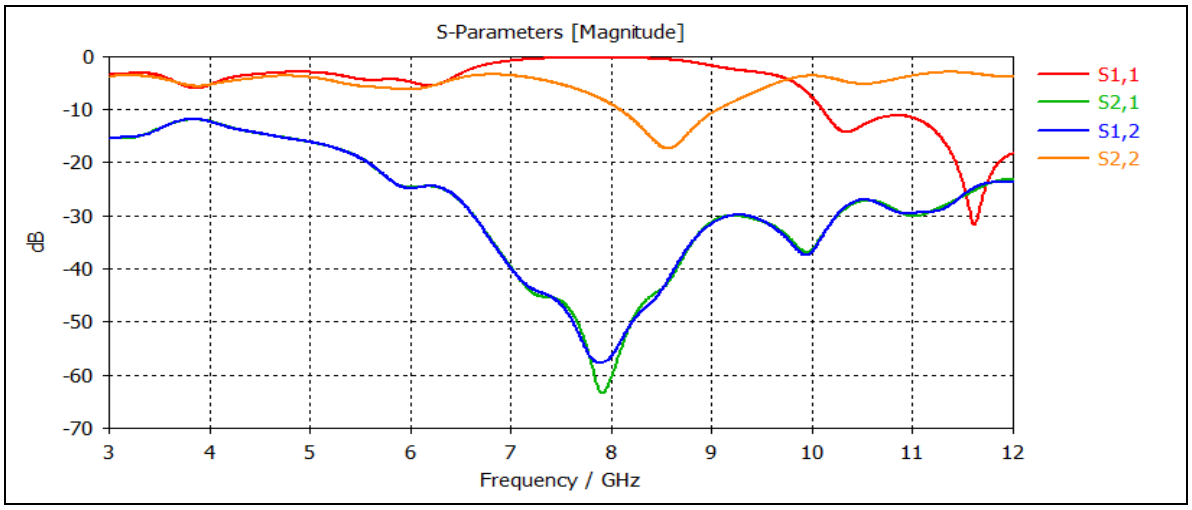

Fig 15 Simulated S-parameters: (a) Reflection Coefficient Magnitude |S11|, (b) Mutual Coupling |S21| Between Antenna Elements.

➢ *MIMO Diversity Performance*

The MIMO diversity metrics, illustrated in Fig. 16, demonstrate exceptional performance across all evaluated criteria. The ECC remains well below the 0.5 threshold, attaining a minimum value of 0.0113. The Diversity Gain approaches the theoretical maximum of 10 dB, achieving 9.998 dB for the optimal configuration. The CCL remains negligible, with maximum value 0.0037 bits/s/Hz significantly below the 0.4 bits/s/Hz threshold.

ISSN No:-2456-2165 https://doi.org/10.38124/ijisrt/26apr1449

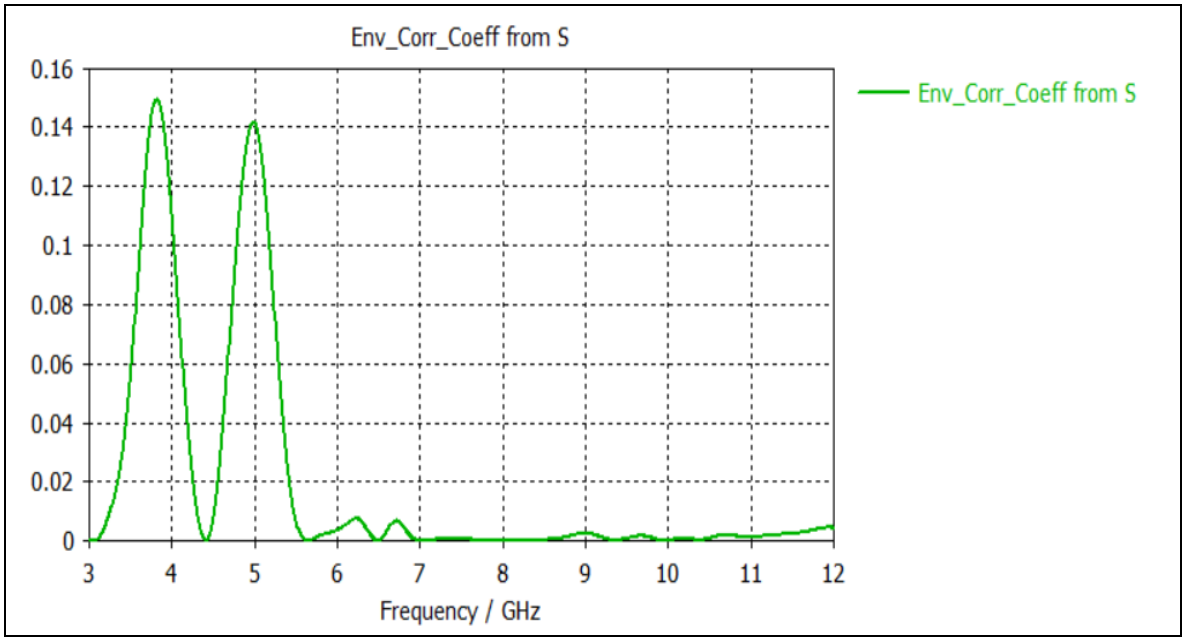

Fig 16 MIMO Diversity Performance Metrics: (a) Envelope Correlation Coefficient, (b) Diversity Gain, (c) Channel Capacity Loss.

Table 3 Summarizes the MIMO Performance Metrics Compliance.

Table 3 MIMO Performance Metrics Compliance

Metric	Specification	Achieved	Margin
ECC	< 0.5	0.0137	97.3%
DG	~ 10 dB	9.996 dB	99.96%
CCL	< 0.4 bits/s/Hz	0.0011	99.7%
Isolation	< −15 dB	−29.72 dB	98.1%

➢ *Surrogate Model Validation*

The machine learning surrogate models demonstrate exceptional predictive accuracy. Gaussian Process Regression achieves R^2 = 0.94 on the training set, while Random Forest Regression attains R^2 = 0.96. Feature importance analysis reveals that the overall scaling parameter x contributes 38% to the response variance, followed by the fractal scale factor a (35%) and feed width wf (27%).

➢ *Optimization Algorithm Comparison*

Table 4 presents the comparative performance of the four optimization strategies. The MFO-GPR combination emerges as the superior methodology, achieving the optimal fitness value of −8.76 and the lowest ECC of 0.0137.

Table 4 Optimization Strategy Comparison

Method	S11 (dB)	Isolation (dB)	ECC	DG (dB)	Fitness
PSO+GPR	−6.93	−30.75	0.0173	9.992	−8.14
PSO+RFR	−6.88	−30.98	0.0190	9.991	−7.89
MFO+GPR	**−6.78**	**−29.72**	**0.0137**	**9.996**	**−8.76**
MFO+RFR	−3.21	−37.23	0.0139	9.992	−6.52

The optimized design parameters identified through the MFO-GPR methodology are: x = 12.35 mm, wf = 3.12 mm, and a = 3.45 mm.

➢ *Optimized Design Characterization*

The MFO-GPR optimized configuration achieves exceptional performance metrics: $|S_{11}|$ = −6.78 dB, ECC = 0.0137, DG = 9.996 dB, CCL = 0.0011 bits/s/Hz, and isolation of −29.72 dB. Fig. 17 presents the reflection coefficient comparison between initial unoptimized and optimized designs, demonstrating substantial improvement in impedance matching characteristics.

ISSN No:-2456-2165 https://doi.org/10.38124/ijisrt/26apr1449

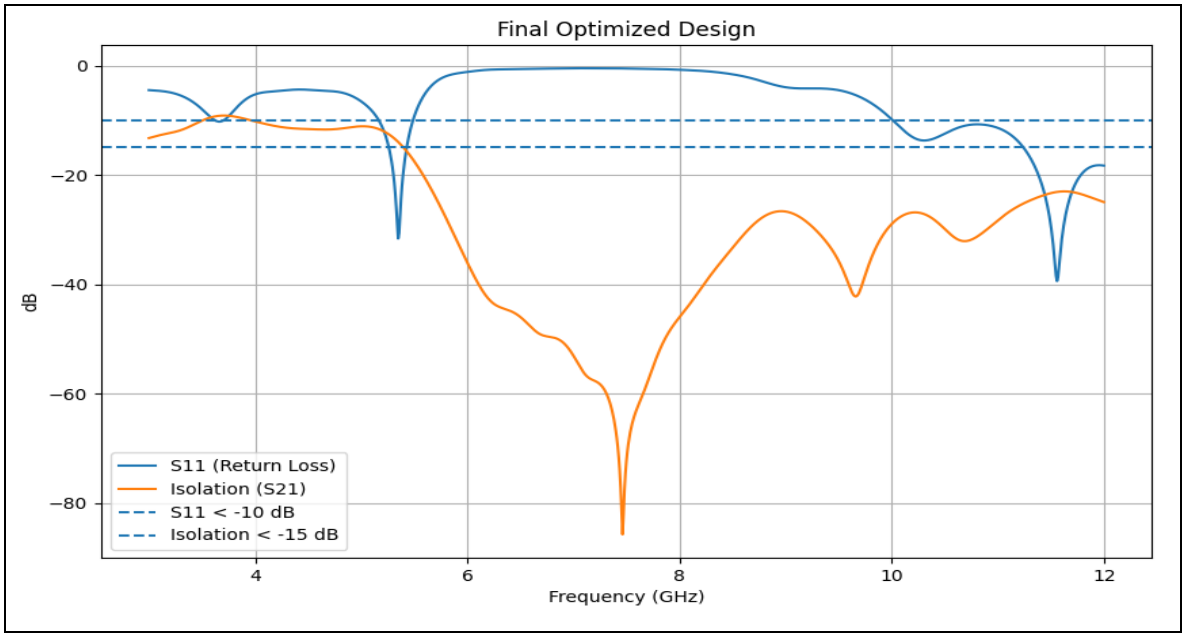

Fig 17 Reflection Coefficient Comparison: Initial Unoptimized Design Versus MFO+GPR Optimized Design Showing Improvement in Impedance Matching.

➢ *Radiation Characteristics*

The far-field radiation pattern, illustrated in Fig. 18, exhibits stable characteristics across the operational bands. The pattern demonstrates adequate directivity and symmetric radiation, confirming suitability for wireless communication applications.

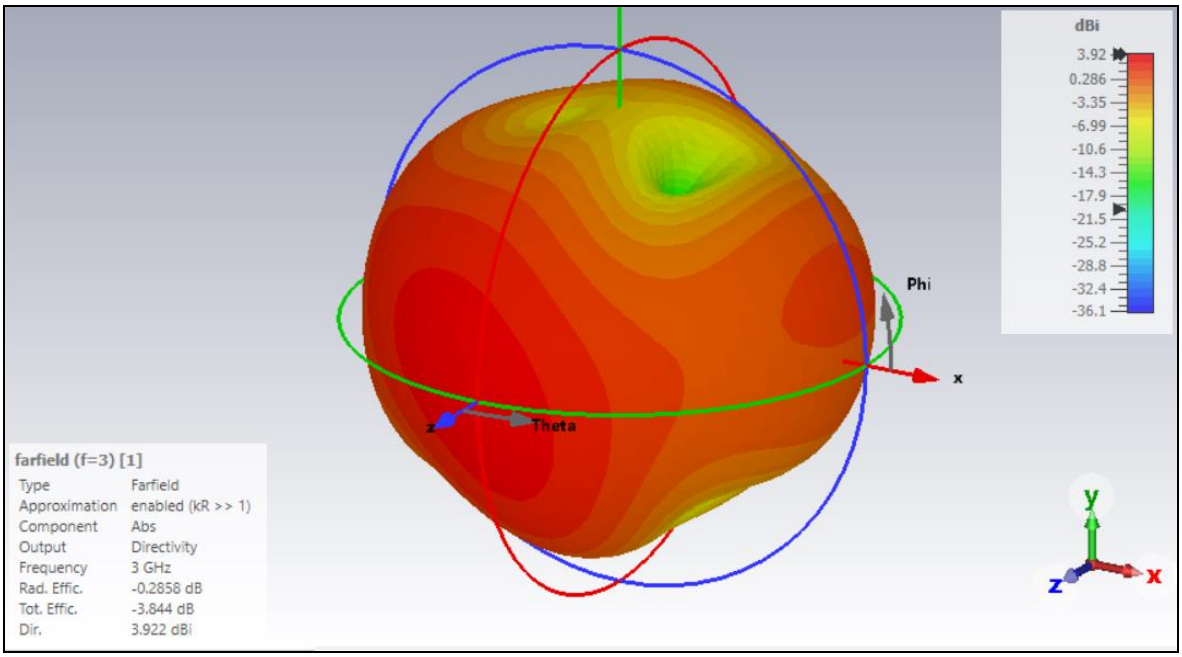

Fig 18 Simulated Far-Field Radiation Pattern at Resonant Frequencies: (a) E-plane, (b) H-plane.

➢ *Computational Efficiency Analysis*

The surrogate-assisted optimization framework achieves remarkable computational efficiency. The traditional parameter sweep approach would require approximately 66.7 hours, whereas the proposed methodology completes in 1.6 hours—a reduction of 97.6%. This acceleration is realized through the combination of limited training data (20 simulations) and rapid surrogate model evaluation (milliseconds per prediction).

V. CONCLUSION AND FUTURE DIRECTIONS

➢ *Principal Achievements*

This manuscript has presented the design and machine learning-assisted optimization of a fractal-based multi-band MIMO antenna. The principal achievements include:

- Successful realization of a Koch snowflake-inspired multi-band MIMO topology achieving concurrent

ISSN No:-2456-2165 https://doi.org/10.38124/ijisrt/26apr1449

operation across multiple frequency bands within compact volumetric constraints.
- Rigorous validation of GPR and RFR surrogate methodologies, achieving R^2 = 0.94 and R^2 = 0.96, respectively.
- Demonstrated superiority of the MFO-GPR methodology, achieving optimal fitness value −8.76 and lowest ECC of 0.0137.
- Achievement of 97.6% reduction in computational time, reducing design cycle duration from 66.7 hours to 1.6 hours.

➢ *Performance Synopsis*

The optimized multi-band MIMO antenna exhibits exceptional diversity performance:

- ECC: 0.0137 (97.3% margin below threshold)
- DG: 9.996 dB (99.96% of theoretical maximum)
- Isolation: −29.72 dB (excellent decoupling)
- CCL: 0.0011 bits/s/Hz (negligible capacity degradation)

➢ *Limitations and Constraints*

The present investigation is subject to certain limitations. The results are predicated upon computational electromagnetic simulation, and fabrication tolerances may introduce deviations between simulated and measured performance. Environmental factors including temperature and humidity variations have not been explicitly modeled. Experimental validation through prototype fabrication and measurement remains pending.

➢ *Future Research Trajectories*

- Experimental Validation: Fabrication of physical prototypes and comprehensive measurement campaigns.
- MIMO Configuration Expansion: Extension to 4×4 MIMO configurations for enhanced spatial multiplexing capacity.
- Deep Learning Integration: Investigation of Convolutional Neural Networks (CNN) and LSTM architectures for improved surrogate modeling accuracy.
- Multi-Objective Optimization: Implementation of NSGA-III and MOEA/D for Pareto-optimal design exploration.
- Wearable Application Compliance: Assessment of Specific Absorption Rate (SAR) characteristics for body-worn applications.

REFERENCES

[1]. A. Goldsmith, S. A. Jafar, N. Jindal, and S. Vishwanath, "Capacity limits of MIMO channels," IEEE J. Sel. Areas Commun., vol. 21, no. 5, pp. 684–702, June 2003.
[2]. B. B. Mandelbrot, The Fractal Geometry of Nature. San Francisco, CA: Freeman, 1982.
[3]. Q. Liu, Y. Liu, J. Gao, and M. Li, "Machine learning-assisted optimization for antenna design," IEEE Trans. Antennas Propag., vol. 71, no. 3, pp. 2573–2583, Mar. 2023.
[4]. C. P. Baliarda, J. Romeu, and A. Cardama, "The Koch monopole: A small fractal antenna," IEEE Trans. Antennas Propag., vol. 48, no. 11, pp. 1773–1781, Nov. 2000.
[5]. J. Kennedy and R. Eberhart, "Particle swarm optimization," in Proc. IEEE Int. Conf. Neural Networks, Perth, Australia, 1995, pp. 1942–1948.
[6]. S. Mirjalili, "Moth-flame optimization algorithm: A novel nature-inspired heuristic paradigm," Knowl.-Based Syst., vol. 89, pp. 228–249, Nov. 2015.
[7]. C. E. Rasmussen and C. K. I. Williams, Gaussian Processes for Machine Learning. Cambridge, MA: MIT Press, 2006.
[8]. L. Breiman, "Random forests," Mach. Learn., vol. 45, no. 1, pp. 5–32, Oct. 2001.
[9]. R. Ghatak, D. R. Poddar, and R. K. Mishra, "Wideband Koch fractal antennas," Int. J. RF Microw. Comput.-Aided Eng., vol. 24, no. 1, pp. 56–62, Jan. 2014.
[10]. D. H. Werner and S. Ganguly, "An overview of fractal antenna engineering research," IEEE Antennas Propag. Mag., vol. 45, no. 1, pp. 38–57, Feb. 2003.
[11]. H. H. Chou et al., "Machine learning-assisted antenna design: A comprehensive review," IEEE Access, vol. 9, pp. 59330–59343, 2021.
[12]. C. A. Balanis, Antenna Theory: Analysis and Design, 4th ed. Hoboken, NJ: Wiley, 2016.
[13]. R. Kumar and S. B. Rana, "Design and analysis of compact UWB-MIMO antenna with enhanced isolation," AEU-Int. J. Electron. Commun., vol. 162, p. 154565, Jan. 2023.
[14]. P. Sharma, A. Gupta, and R. K. Singh, "Fractal-based multi-band antenna for 5G applications," IEEE Trans. Circuits Syst. II, vol. 71, no. 8, pp. 3456–3460, Aug. 2024.
[15]. L. Zhang and Y. Wang, "Machine learning-optimized compact MIMO antenna for wireless applications," IEEE Open J. Antennas Propag., vol. 6, pp. 112–125, 2025.
[16]. J. Liu, S. Xie, and Y. Liu, "Isolation enhancement in MIMO antennas: A review," IEEE Access, vol. 4, pp. 2518–2526, 2016.
[17]. M. A. S. Masoud et al., "Wideband MIMO antenna with high isolation using metamaterial decoupling," IEEE Antennas Wireless Propag. Lett., vol. 23, no. 2, pp. 412–416, Feb. 2024.
[18]. CST Studio Suite 2025, Dassault Systèmes, "Computer Simulation Technology," 2025.
[19]. K. Deb and H. Jain, "An evolutionary many-objective optimization algorithm using reference-point-based nondominated sorting approach," IEEE Trans. Evol. Comput., vol. 18, no. 4, pp. 577–601, Aug. 2014.
[20]. Y. Wang, X. Chen, and Z. Li, "Deep learning surrogate models for electromagnetic optimization," IEEE Trans. Microw. Theory Techn., vol. 72, no. 5, pp. 2789–2801, May 2024.